Geomechanics and Engineering, *Vol. 27, No. 3 (2021) 223-237*
https://doi.org/10.12989/gae.2021.27.3.223

Study on the packing and shear characteristics of granular mixtures via the DEM

Jian Gong[1,2], Lipo Cheng[1], Lianheng Zhao[2], Jinfeng Zou[2], Liang Li[2] and Zhihong Nie*[2]

[1]*College of Civil Engineering and Architecture, Guangxi University, Guangxi, China*
[2]*School of Civil Engineering, Central South University, Hunan, China*

(Received March 21, 2019, Revised January 1, 2021, Accepted October 12, 2021)

Abstract. Granular mixtures are often encountered in civil engineering, but the micromechanical implications of their packing and shear characteristics are still unclear. In this study, the packing and shear characteristics of binary mixtures were studied using a three-dimensional discrete element method (DEM). The binary mixtures contained realistic gravel-shaped coarse particles and one of two tested fine particle shapes (namely, spherical or elongated particles). The densest isotropic samples were generated by using a frictionless condition. The initial void ratio and particle contacts of the packed samples were examined. This study shows that the particle shape of the fines affects the relationship between the initial void ratio and fines content (FC). The contact types in binary mixtures can be classified as coarse particle-coarse particle (CC contacts), coarse particle-fine particle (CF contacts) and fine particle-fine particle (FF contacts). A microscopic investigation of the particle contacts indicated that the coarse and fine particle shapes influenced the partial coordination numbers of the CC and CF contacts and the CF and FF contacts, respectively. All the samples were then subjected to numerical triaxial compression tests. The results show that the particle shape of the fines affected the magnitudes and evolutions of the peak (φ_p) and critical (φ_c) friction angles of the binary mixtures. Finally, an anisotropic analysis was performed to highlight the microscopic mechanisms that cause the shear strength to be dependent on the particle shape and FC.

Keywords: discrete element method; granular mixtures; fines content; fine particle shape; packing characteristics; shear strength

1. Introduction

Natural and manmade granular mixtures are often encountered in geotechnical engineering. For example, geomorphological features include mountains and hills that often consist of mixtures of boulders, gravels and sand (Kuenza *et al*. 2004). Engineering structures such as rockfills in cohesionless soil deposits are usually made of a mixture of rock and sand particles (Vallejo 2001). In addition, the rock blocks of mudstone and sandstone, which are excavated from mountains or foundation ditches, are naturally mixed together because of the interbedded deposit structure (Wang *et al*. 2013). Regarding the engineering application or the stability of natural slopes of these granular mixtures, their packing and shear characteristics must be considered. Granular mixtures that consist of two or more types of soils with different shapes and sizes have a distinct structure. Binary mixtures are the simplest case among the mixture packings and are made of coarse and fine particles. Previous theoretical (Weatman 1936, Yin *et al*. 2014, Yu *et al*. 1988) studies have focused on the effect of the coarse (or fine) fraction on the packing void ratio of binary mixtures. In addition, Lade *et al*. (1998) and Vallejo (2001) explore the effect of the fines on the packing void ratio of silty sands and spherical glass beads with different size, respectively. Furthermore, other experimental studies (Kuenza *et al*. 2004, Vallejo 2001, Wei *et al*. 2018, Xu *et al*. 2011, Xu *et al*. 2007, Wang *et al*. 2016) have focused on the effect of the coarse (or fine) fraction on the shear strength of binary mixtures (i.e., Kuenza *et al*. 2004 conducted on gravelly soils; Vallejo (2001) conducted on glass beads with different size; Wei *et al*. 2018, Xu *et al*. 2011, Xu *et al*. 2007 conducted on soil-rock mixtures; Wang *et al*. 2016 conducted on sandstone-mudstone particle mixture). Such theoretical and experimental studies provide a basic macroscale picture of the packing and shear characteristics of granular mixtures. However, this picture is insufficient since the micromechanical implications governed by the contact type, contact force distribution and anisotropic characteristics are still unclear. In fact, the engineering properties of granular mixtures are quite complex, essentially due to their discrete and heterogeneous nature, resulting in a specific internal texture under packing and external loading. Therefore, it is necessary to study the internal texture of granular mixtures to understand the micromechanical implications of their packing and shear characteristics. The experimental devices traditionally used cannot fully depict the microscale properties. Even some advanced and expensive imaging devices, such as X-ray computed tomography (CT) instrumentation, cannot accurately capture the contact force distribution among irregular grains (Hall *et al*. 2010). The discrete element method (DEM) is based on discrete particle mechanics and

*Corresponding author, Professor
E-mail: niezhih@126.com

ISSN: 2005-307X (Print), 2092-6219 (Online)

was introduced by Cundall and Strack (1979); the DEM is an alternative approach to studying the packing and shear characteristics of granular mixtures at both the macroscale and microscale. It has been demonstrated that the DEM can reproduce certain key features of soils and reveal many types of macroscopic soil behaviors at a particulate level, such as the small strain behavior of granular material (Gu *et al*. 2017, Gu *et al*. 2018), the effects of interparticle friction and the particle size on the shear behavior of granular materials (Dai *et al*. 2016, Dai and Yang 2017, Harehdasht *et al*. 2017), monotonic and cyclic behaviors of sands (Gu *et al*. 2020), and the mechanical behavior of asphalt mixtures (Peng *et al*. 2018, Zhang *et al*. 2017).

The macroscopic mechanical behavior of granular materials is governed by microscopic features at the particle scale. It is widely known that the DEM is a powerful and computationally intensive approach used to simulate granular materials. Recently, many DEM studies have been conducted on the packing and shear characteristics of binary mixtures. For example, Minh and Cheng (2013) and Minh *et al*. (2014) studied the force transmission and distribution of interparticle contact forces using a three-dimensional (3D) DEM with frictional spherical particles. Shire and O'Sullivan (2013) and Shire *et al*. (2016) also used spherical particles to simulate binary mixtures using a 3D DEM and investigated the contact distributions, contact forces and transmitted stresses to assess the internal stability of gap-graded soils. Alternatively, Ueda *et al*. (2011), Dai *et al*. (2015, 2019), Gong and Liu (2017a) and Gong and Liu (2019) explored the shear strength transition of densely packed binary mixtures using a two-dimensional (2D) DEM for frictional discoid particles. Zhou *et al*. (2016) prepared a packed binary mixture in the maximum packing efficiency state using a 3D DEM for frictional spherical particles and studied the effect of the particle size ratio on the deviator stress and initial elastic modulus of the binary mixtures. The abovementioned DEM studies commonly used spherical and discoid particles to model particle interactions, considering the expensive computational resources required to simulate a binary mixture system (Berger *et al*. 2014). However, when compared with real particles, the spherical and discoid particles are clearly very simplified. Recently, other researchers have attempted to adopt nonspherical particles in DEM simulations to investigate the mechanical behaviors of binary mixtures. For example, Xu *et al*. (2016) and Lu *et al*. (2017) used polygonal coarse and discoid fine particles to investigate the shear strength, failure process and deformation characteristics of binary mixtures. Azema *et al*. (2016a) adopted elongated coarse and discoid fine particles to study the shear strength and microstructure of binary mixtures by varying the degree of homogeneity. Furthermore, Ng *et al*. (2017) and Ng *et al*. (2018) employed ellipsoidal coarse and fine particles to study the packing density, initial modulus, critical shear strength and particle contacts of binary mixtures with different particle shapes and fines contents (FCs). Polygonal, elongated and ellipsoidal particles alone cannot synthetically reflect the particle shape characteristics of real granular materials. In addition, in previous studies, the effect of the fines particle shape on the packing and shear characteristics of binary mixtures has not yet been investigated. This knowledge gap motivates this work, wherein we conduct binary mixtures consisting of realistic gravel-shaped coarse particles and fines with two shapes using a 3D DEM.

The aim of this study is to systematically explore the packing and shear characteristics of binary mixtures through DEM simulations. A total of 64 realistic gravel-shapes, generated using a multisphere approach, were used to model the coarse particles. Spherical and elongated particles were used to model two types of fines. The main innovation of this work is that the influences of the fine particle shape and content on the void ratio, particle contacts and shear strength of the binary mixtures were carefully examined. The remainder of this paper is organized as follows. First, an introduction of DEM modeling is given. Then, the initial void ratio and particle contacts of the packed samples are investigated. Next, all the packed samples undergo triaxial testing to quantify their peak and critical shear strengths and the influence of the fine particle shape and content on these strengths. Then, the stress-force-fabric relationship is analyzed, and the evolution of any fabric anisotropies affected by the fine particle shape and content is evaluated. Finally, the main conclusions of this study are presented.

2. DEM modeling

2.1 Sample generation and simulation parameters

The numerical simulations were performed by using a well-known 3D DEM code, PFC^{3D} (Itasca 2014). Samples were created by mixing coarse and fine materials. The coarse material reflects the realistic geometries of gravel. The gravel-shaped coarse particles were simulated using a multisphere filling approach, which is a built-in function of PFC^{3D}, described by Taghavi (2011), to determine the positions and radii of the subspheres. The geometries of the gravels were obtained from X-ray CT, which has been demonstrated to be a reliable technique for obtaining the shape characteristics of granular materials to a satisfactory resolution (Wang *et al*. 2007). The CT scanning of gravels provides data in STL files that can be utilized by PFC^{3D} (Itasca 2014). Note that an STL file stores a triangular surface mesh used by the rapid prototyping industry as a standard file format. The STL files were then filled with subspheres to create the coarse particles. Figs. 1(a)-(c) illustrate an example of the real gravels, the triangular surfaces stored in the STL files and the corresponding sphere-filled gravel-shaped particles, respectively. A comparison of Fig. 1(a) and Fig. 1(c) indicates that the geometries of the gravel-shaped particles are similar to those of the real gravels. Figs. 2(a) and 2(b) present the coarse and fine particles used to simulate the binary mixtures in this study, respectively. As illustrated in Fig. 2(a), 64 gravel-shaped particles are used to simulate the coarse component material. Each number in the sub-box represents the corresponding number of subspheres used to fill the particle and is controlled by two parameters of the particle shape description (namely, *distance* and *ratio*), as

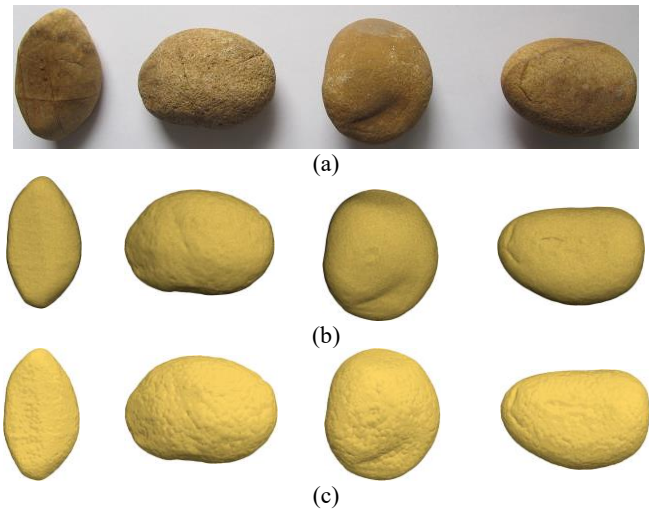

Fig. 1 (a) Real gravels; (b) STL file of the scanned gravel; (c) gravel-shaped particle generation by filling the STL file with sub-spheres

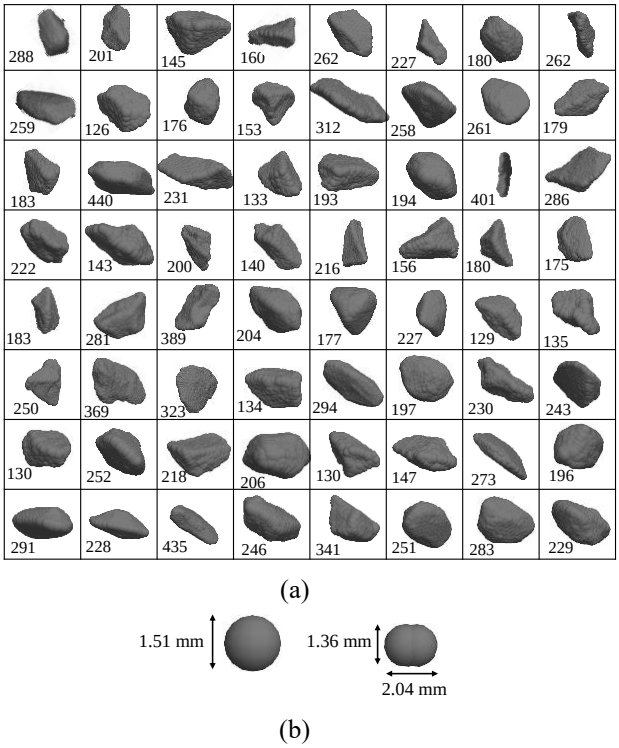

Fig. 2 Coarse and fine particles used to model the gravel-fine mixture: (a) the 64 types of gravel-shaped particles used to simulate the coarse material as distance = 150 and ratio = 0.3, and the number in the sub-box represents the corresponding number of sub-spheres; (b) spherical and elongated particles used to simulate fine material, with ARs are 1.0 and 1.5, respectively

defined by Taghavi (2011). The *distance* is used to describe an angular measure of the particle smoothness in degrees, from 0 to 180. The greater the *distance* is, the smoother the subsphere distribution. The *ratio* indicates the ratio of the smallest to largest subsphere radius in the particle, with 0 < *ratio* <1. In general, the greater the *distance* and the smaller the *ratio* in our multisphere approach, the greater the number of subspheres required to fill the gravel-shaped particle. In this study, the *distance* and *ratio* of all the coarse particles are adopted as 150 and 0.3, respectively, the same values as those used in Gong and Liu (2017b) to investigate the shear responses of a packed multisphere ellipsoid. As indicated in Fig. 2(b), spherical and elongated fines are adopted to study the effect of the particle shape of fines on the packing and shear characteristics of binary mixtures. The aspect ratios (ARs) of the spherical and elongated fines are 1.0 and 1.5, respectively.

To generate a sample, particles shown in Fig. 2(a) are randomly selected as the coarse particles. All the coarse particles have the same volume, equal to the volume of an equivalent sphere with a diameter D_c of 6.72 mm, which is the average diameter of the scanned gravels. The diameters of the fines with different particle shapes D_f are set to 1.51 mm. Accordingly, the particle size ratio $\alpha = D_c/D_f = 4.44$. Based on crystallography, the maximum diameter of a sphere that can occupy the smallest void in the densest possible packing of equal-sized spheres of diameter D is D/4.44 (Krishna *et al*. 1981). Thus, the particle size ratio α = 4.44 used in this study is considered high enough to ensure that fines occupy the voids within a dense packing of coarse particles without greatly disrupting its skeleton. Note that α = 4.44 was also adopted in previous numerical simulations (De Frias Lopez *et al*. 2016a, De Frias Lopez *et al*. 2016b) to study the resilient properties, force transmission and soil fabric of granular mixtures. In addition, α = 4.44 has been suggested to define the limit for interacting fractions in pavement design (e.g., Yideti *et al*. 2013, Guarin *et al*. 2013). Samples with FCs ranging from 0% to 100% were generated in steps of 10%. For convenience, each sample is identified by the content and particle shape of its fines. For example, FC100-AR1.0 represents the sample with a FC of 100% (pure fine particles) and a fines AR of 1.0 (i.e., sphere). FC50-AR1.5 indicates the sample with a FC of 50% and a fines AR of 1.5 (i.e., elongated particles). The number of coarse particles N_{cp} is first determined when generating a sample; then, the number of fine particles N_{fp} can be calculated by the specific FC and the given particle density. The N_{cp} value of each sample is the same as that used in Minh *et al*. (2014), who studied the contact force distribution of granular mixtures using a 3D DEM. Note that greater N_{cp} values may be more realistic, but the corresponding simulation requires more computational resources. Initially, coarse and fine particles were generated with random orientations and zero contacts within a cube. To avoid force gradients and obtain dense isotropic samples, the gravitational acceleration and friction coefficients of the particles were temporarily set to zero. Generally, a friction coefficient of zero during sample generation can produce the densest assembly for a given generation procedure (Abbireddy *et al*. 2010). Frictionless conditions were also adopted in previous studies of DEM simulations of binary mixtures (e.g., Azema *et al*. 2016b, Gong *et al* 2019, Gong and Liu 2017a, Minh *et al*. 2014). The samples were then subjected to isotropic compression at a low strain rate. A servo-controlled mechanism was introduced to maintain the

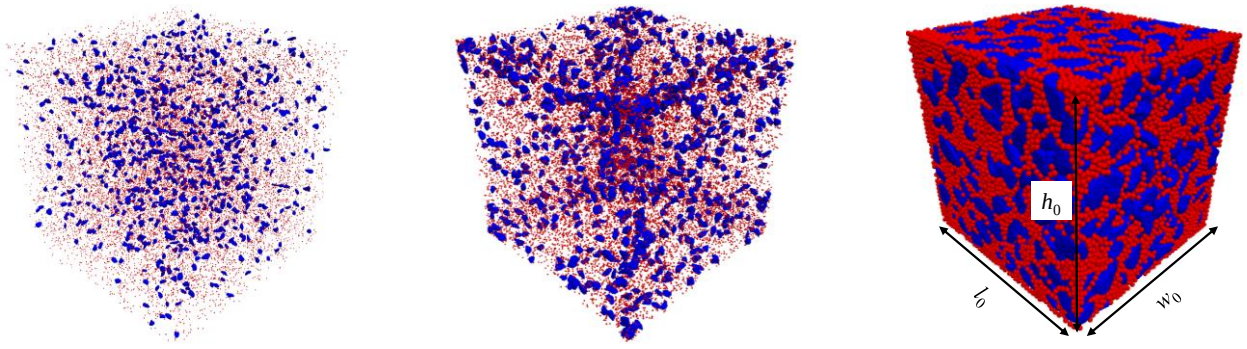

(a) (b) (c)

Fig. 3 Snapshots of FC20-AR1.5 during the compression phase: (a) initial stage; (b) intermediate stage; (c) final stage. Blue particles represent the coarse particles and red particles indicate the fines

desired confining pressure of σ_c = 200 kPa during the isotropic compression (Itasca 2014). The sample was considered to be in equilibrium when the ratio of the mean static unbalanced force to the mean contact force was less than 10^{-5}, and the stress obtained from the walls to σ_c was smaller than a tolerance of 0.5%. Snapshots of FC20-AR1.5 during the compression phase are illustrated in Fig. 3: (a) initial stage; (b) intermediate stage; and (c) final stage. The l_0, w_0 and h_0 parameters in the final stages indicate the length, width and height, respectively, of the packed sample before shear. After isotropic compression, the initial void ratios of the packed samples (e_0) were measured, and the particle-particle friction coefficients μ were set to 0.5 for the shear testing. Note that no calibration was performed and all the parameter values were taken from literatures. For example, μ = 0.5 was used in many previous DEM studies (e.g., Guo and Zhao, 2013, Gong and Liu 2017a, Gong and Liu 2017b). Gong *et al*. (2019b) used multisphere ellipsoids to study the effect of μ value on the shear strengths of cohesionless granular materials and found that as the μ value increase, peak shear strength gradually increases while critical shear strength first increases with μ and then reaches a plateau when $\mu \geq 0.3$.

The contacts were simulated by using a soft contact model with a specified contact deformation relationship. A simple linear elastic contact model was used for the interparticle and particle-wall interactions, and a contact slip was introduced according to the Coulomb friction law. The ability of the linear elastic contact model to reproduce certain key features of granular mixtures has previously been demonstrated (e.g., Dai *et al*. 2015, De Frias Lopez *et al*. 2016a, De Frias Lopez *et al*. 2016b, Gong *et al*. 2019a, Gong and Liu 2017a, Minh *et al*. 2014). The microscopic parameters used in the simulations are listed in Table 1. The normal contact stiffness of the interparticle k_n varies according to $k_n = 2rE_c/(r_a+r_b)$, where E_c denotes the contact effective modulus, r_a and r_b denote the radii of the particles in contact, and r represents the smaller value between r_a and r_b. The values of E_c in this study are consistent with those reported in Gong and Liu (2017b), who simulated the response of multisphere ellipsoid samples. The k_n/k_s value (where k_s denotes the shear contact stiffness of the subsphere) suggested by Goldenberg *et al*. (2005) for realistic granular materials is in the range of $1.0 < k_n/k_s < 1.5$. Hence, $k_n/k_s = 4.0/3$ was adopted in this study.

Table 1 Input parameters in the DEM simulations

Parameter	Value
Particle density, ρ	2600 kg/m^3
Inter-particle friction, μ	0.5
Wall-particle friction, μ_w	0.0
Contact modulus of particle-wall	1×10^9 Pa
Contact modulus of interparticle	1×10^8 Pa
k_n/k_s	4/3
Damping constant	0.7

2.2 Details of the experimental program

The contact types in binary mixtures can be classified as coarse particle-coarse particle (CC contacts), coarse particle-fine particle (CF contacts) and fine particle-fine particle (FF contacts). In this study, the partial coordination number of each contact type is explored. The details of the experimental program for the packed binary mixtures are listed in Table 2, which includes the FC, sample dimension ratio, total number of particles, contact numbers of each contact type, number of rattler particles and e_0 values. N_{cp}, $N_{cp\text{-}sub}$ and N_{fp} represent the number of coarse particles, number of subspheres constituting the coarse particles and number of fine particles, respectively. A high number of fines (i.e., N_{fp}) results in high computational expenses. A workstation with an Intel®Xeon® CPU E5-2690v4(×2) was used to conduct the numerical simulations in this study, and the average calculation time of each DEM numerical test was approximately 25 days. Jamiolkowski *et al*. (2004) suggests that the ratio of the sample size to the maximum particle size should be greater than 5, with an ideal ratio of 8, to eliminate the effect of the sample size and minimize stress nonuniformities inside a sample. In Table 2, the minimum ratios of $D^{\#}/D_c$ ($D^{\#}$ = min(h_0, w_0, l_0)) approach 8.82 for FC30-AR1.0 and 8.86 for FC70-AR1.5. N_c^{CC}, N_c^{CF} and N_c^{FF} indicate the total numbers of the CC, CF and FF contacts, respectively (not between constituent subspheres). Numerical simulations of binary mixtures have revealed that there are many rattler particles that have no contacts or only one contact. N_{cr1}^{CC}, N_{cr1}^{CF} and N_{cr1}^{FF} represent the numbers of rattlers with only one contact for each contact type. In addition, N_{rp0} denotes the number of rattlers with no

Table 2 Fines content, sample dimension ratios, particle numbers, contact numbers of each contact type, rattler particles and initial void ratio of the packed binary mixtures

Samples	$D^{\#}/D_c$	N_{cp}/N_{fp}	$N_{cp\text{-}sub}$	$N_c^{CC}/N_c^{CF}/N_c^{FF}$	$N_{cr1}^{CC}/N_{cr1}^{CF}/N_{cr1}^{FF}$	N_{rp0}	e_0
FC0-AR1.0	9.04	2000/0	381126	8341/0/0	0/0/0	0	0.531
FC10-AR1.0	9.03	971/9560	185064	3685/4748/2176	0/76/78	6714	0.443
FC20-AR1.0	8.96	855/18838	162032	3027/14878/14359	0/100/223	7444	0.372
FC30-AR1.0	8.82	749/28300	141614	2275/25922/39765	0/133/290	3820	0.354
FC40-AR1.0	9.10	642/37695	121559	1406/32194/78021	0/16/57	1192	0.378
FC50-AR1.0	9.24	535/47127	101219	894/30207/107562	0/16/107	1021	0.407
FC60-AR1.0	9.25	427/56421	80206	676/30308/144170	0/2/18	896	0.438
FC70-AR1.0	9.37	320/65586	59976	251/22624/181777	0/3/36	749	0.479
FC80-AR1.0	9.35	210/74458	39250	87/15499/214536	0/3/64	667	0.513
FC90-AR1.0	9.40	104/82974	19136	26/7839/248684	0/1/63	636	0.543
FC100-AR1.0	20.09[a]	0/10000	0	0/0/31503	0/0/0	92	0.587
FC0-AR1.5	8.99	2000/0	381126	8341/0/0	0/0/0	0	0.531
FC10-AR1.5	9.15	971/9484	184962	3782/2812/1015	0/31/21	8050	0.438
FC20-AR1.5	9.11	855/18816	164378	3002/17009/19450	0/73/144	6264	0.354
FC30-AR1.5	9.12	749/28263	141013	2221/33381/56905	0/25/43	1503	0.328
FC40-AR1.5	9.01	642/37675	121559	1582/36884/95840	0/8/15	511	0.335
FC50-AR1.5	8.95	535/47057	101036	1010/36838/136677	0/4/7	216	0.346
FC60-AR1.5	8.92	427/56333	80806	601/32849/180249	0/2/5	135	0.363
FC70-AR1.5	8.86	320/65331	59793	316/26246/225317	0/1/3	84	0.383
FC80-AR1.5	9.06	210/74432	39468	149/18233/267686	0/0/4	47	0.407
FC90-AR1.5	9.22	104/82846	19354	34/9687/314393	0/0/2	57	0.427
FC100-AR1.5	19.66[*]	0/10000	0	0/0/38679	0/0/0	11	0.463

[a]$D^{\#}/D_f$ is 20.09 for FC100-AR1.0 and 19.66 for FC100-AR1.5, where $D^{\#}$ denotes min(h_0,l_0,w_0)and D_f =1.51 mm represents the particle diameter of fines

contacts. The conventional overall coordination number Z_o can be defined as $2N_{tc}/N_{tp}$, where N_{tc} ($=N_c^{CC}+N_c^{CF}+N_c^{FF}$) is the total number of contacts and N_{tp} ($=N_{cp}+N_{fp}$) is the total number of particles in the samples. None of the rattlers contribute to the stable state of stress (Thornton 2000). Hence, a mechanical coordination number Z_m is defined as follows:

$$Z_m = \frac{2[N_{tc} - (N_{cr1}^{CC} + N_{cr1}^{CF} + N_{cr1}^{FF})]}{N_{tp} - N_{rp0} - 2(N_{cr1}^{CC} + N_{cr1}^{CF} + N_{cr1}^{FF})} \quad (1)$$

3. Packing characteristics

Based on the initial void ratio (e_0) in Table 2, Fig. 4 displays the relationship between e_0 and FC for all the samples. The two types of mixtures show a trend in which e_0 first decreases and then increases with increasing FC. The e_0 versus FC curve thus has a 'V' shape, which compares well with other numerical results (De Frias Lopez *et al*. 2016a, De Frias Lopez *et al*. 2016b, Minh *et al*. 2014, Ng *et al*. 2017) and experimental observations (Lade *et al*. 1998, Vallejo 2001). The tendency is physically described as follows: for a low FC, the introduction of fines fills the voids developed by the coarse particles, resulting in a decrease in the void ratio; this trend will continue until a minimum void ratio is reached at FC ≈ 30%, beyond which fines tend to separate the coarse particles, gradually leading to an increasing void ratio. At a given FC, e_0 of the spherical fines is greater than that of the elongated fines, indicating that the particle shape of the fines affects the e_0 of the binary mixtures. This is related to the fact that slight deviations from a spherical shape have a strong space-filling effect on the packing of granular materials (Azema *et al*. 2010a). The FC marking this transition in void ratio appears to be approximately 30%, which can be roughly regarded as the threshold FC (FC_{th}) of the binary mixtures. FC_{th} is an indicator for natural mixed soils varying from coarse-dominated to coarse-fine-interaction materials (Polito *et al*. 2001, Thevanayagam *et al*. 2002, Vallejo 2001, Yang *et al*. 2006).

The overall coordination number or number of contact points per particle is an important parameter describing the geometrical arrangement of particles in a packed mixture and is widely used in the evaluation of the structural properties related to the connectivity between particles. In binary mixtures, the mechanical coordination number can be related to the contact type (i.e., partial coordination number) and calculated in a manner similar to that of Z_o (Minh and Cheng 2013):

Table 3 Characteristics of samples of binary mixtures

Samples	Z_o	Z_m	$Z_{CC}^m/Z_{CF}^m/Z_{CF}^m$	$\chi_{CC}/\chi_{CF}/\chi_{FF}$	N_{RP}/N_{TP}
FC0-AR1.0	8.34	8.34	8.34/0.00/0.00	100.00%/0.00%/0.00%	0.00%
FC10-AR1.0	2.03	6.05	7.59/0.89/0.44	34.73%/44.75%/20.51%	67.01%
FC20-AR1.0	3.28	5.51	7.08/1.50/1.50	9.38%/46.11%/44.50%	41.07%
FC30-AR1.0	4.68	5.54	6.07/1.78/2.79	3.34%/38.14%/58.51%	16.06%
FC40-AR1.0	5.82	6.03	4.38/1.68/4.14	1.26%/28.84%/69.90%	3.49%
FC50-AR1.0	5.82	5.97	3.34/1.27/4.56	0.64%/21.78%/77.57%	2.65%
FC60-AR1.0	6.16	6.26	3.17/1.07/5.11	0.39%/17.30%/82.31%	1.64%
FC70-AR1.0	6.21	6.29	1.57/0.69/5.54	0.12%/11.06%/88.82%	1.25%
FC80-AR1.0	6.16	6.23	0.83/0.42/5.76	0.04%/6.74%/93.22%	1.07%
FC90-AR1.0	6.18	6.23	0.50/0.19/5.99	0.01%/3.06%/96.93%	0.92%
FC100-AR1.0	6.31	6.36	0.00/0.00/6.31	0.00%/0.00%/100.00%	0.92%
FC0-AR1.5	8.34	8.34	8.34/0.00/0.00	100.00%/0.00%/0.00%	0.00%
FC10-AR1.5	1.46	6.56	7.79/0.53/0.21	49.70%/36.96%/13.33%	77.97%
FC20-AR1.5	4.01	6.05	7.02/1.72/2.05	7.61%/43.10%/49.29%	34.05%
FC30-AR1.5	6.38	6.75	5.93/2.30/4.02	2.40%/36.08%/61.52%	5.65%
FC40-AR1.5	7.01	7.11	4.93/1.92/5.09	1.18%/27.46%/71.36%	1.45%
FC50-AR1.5	7.33	7.37	3.78/1.55/5.81	0.58%/21.11%/78.31%	0.50%
FC60-AR1.5	7.53	7.55	2.81/1.16/6.40	0.28%/15.37%/84.35%	0.26%
FC70-AR1.5	7.65	7.66	1.98/0.80/6.90	0.13%/10.42%/89.45%	0.14%
FC80-AR1.5	7.66	7.67	1.42/0.49/7.19	0.05%/6.37%/93.58%	0.07%
FC90-AR1.5	7.81	7.82	0.65/0.23/7.59	0.01%/2.99%/97.00%	0.07%
FC100-AR1.5	7.74	7.74	0.00/0.00/7.74	0.00%/0.00%/100.00%	0.11%

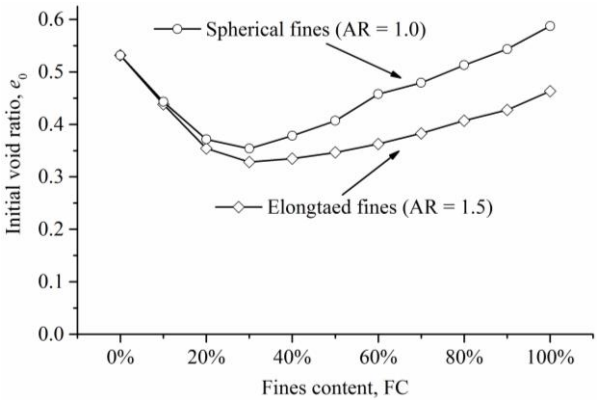

Fig. 4 Evolution of e_0 with respect to FC

$$Z_{CC}^m = \frac{2N_{mc}^{CC}}{N_{cp}}; \quad Z_{CF}^m = \frac{2N_{mc}^{CF}}{N_{tp}}; \quad Z_{FF}^m = \frac{2N_{mc}^{FF}}{N_{fp}} \tag{2}$$

where $N_{mc}^{CC} = N_c^{CC} - N_{cr1}^{CC}$, $N_{mc}^{CF} = N_c^{CF} - N_{cr1}^{CF}$ and $N_{mc}^{FF} = N_c^{FF} - N_{cr1}^{FF}$ are the mechanical contact numbers of the CC, CF and FF contacts, respectively. Table 3 shows the overall, mechanical and partial coordination numbers of the two types of mixtures. Table 3 also includes the mechanical contact number of the CC, CF and FF contacts normalized by the total number of contacts (χ_{CC}, χ_{CF} and χ_{FF}, which are listed in the fifth column) and the proportion of rattler particles to total particles (N_{RP}/N_{TP}, which is listed in the sixth column).

Fig. 5 illustrates the evolutions of Z_o and Z_m with respect to FC for the two mixture types. Similar general trends are observed; both Z_o and Z_m first decrease and then increase, eventually stabilizing. All the curves present a trough, which is consistent with the results in the literature (e.g., Suzuki *et al*. 1999, Kristiansen *et al*. 2005, Meng *et al*. 2014, Suzuki *et al*. 1999). For a given mixture, Z_m is generally greater than Z_o, especially at FCs of 10%-30%. This result is related to the effect of the rattler particles. Table 3 shows that the N_{RP}/N_{TP} values are low except for samples with FCs of 10%-30%. For elongated fines, greater values of Z_o and Z_m are found than those of spherical fines, possibly attributable to the lower initial void ratios, as shown in Fig. 4. Fig. 6 shows the evolutions of Z_{CC}^m, Z_{CF}^m and Z_{FF}^m with respect to FC for the two types of mixtures. As expected, Z_{CC}^m continually decreases and Z_{FF}^m continually increases as the FC increases. The Z_{CF}^m value first increases with increasing FC, reaches a maximum at FC = 30% and then decreases with a further increase in FC. Similar observations were obtained through experiments conducted by Pinson *et al*. (1998). These results are also consistent with previous numerical simulations (e.g., Biazzo *et al*. 2009, Meng *et al*. 2014, Ng *et al*. 2018). When comparing Z_{CC}^m, Z_{CF}^m and Z_{FF}^m between the two types of mixtures, the values of Z_{CC}^m are similar, indicating that Z_{CC}^m is not a function of the fine particle shape. However, the Z_{CF}^m values of the mixtures with elongated fines are slightly greater than those with spherical fines, especially at FC ≤

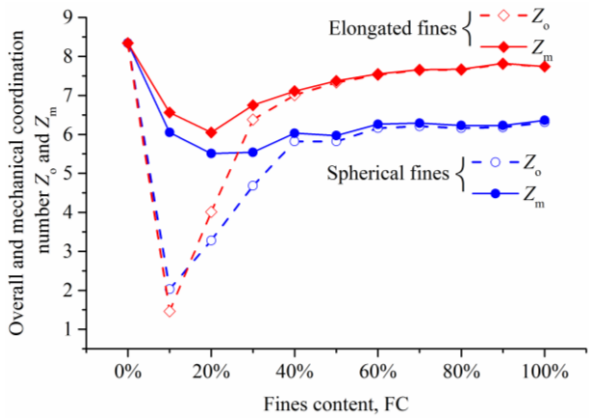

Fig. 5 Evolutions of Z_0 and Z_m with FC for the two types of mixtures

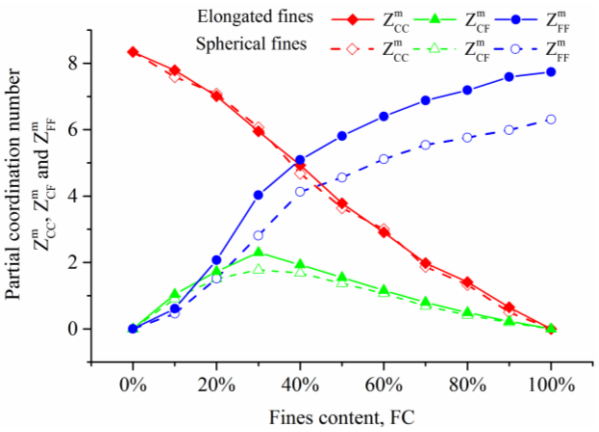

Fig. 6 Evolutions of Z_{CC}^m, Z_{CF}^m and Z_{FF}^m with respect to FC for the two types of mixtures

30%. In addition, for all the values of FC tested, Z_{FF}^m of the mixtures with elongated fines are greater than those with spherical fines. Since the numbers of coarse and fine particles in the samples with different fine particle shapes are generally identical, the results should be related to the number of CF and FF contacts. This relationship is evident in Table 2; the particle shape of the fines influences the numbers of CF and FF contacts but has a limited effect on the number of CC contacts.

Previous studies have focused on the partial coordination numbers of spherical or ellipsoidal binary mixtures. For example, Pinson *et al*. (1998) experimentally studied the partial coordination numbers of binary mixtures of steel balls by using the liquid bridge technique. Rodriguez *et al*. (1986), Biazzo *et al*. (2009) and Meng *et al*. (2014) numerically investigated the partial coordination numbers of spherical binary mixtures. In addition, Ng *et al*. (2018) recently used ellipsoids with different ARs to explore the partial coordination numbers of binary mixtures. Figs. 7(a)-(c) illustrate the evolution of Z_{CC}^m, Z_{CF}^m and Z_{FF}^m with respect to FC, respectively, and show the experimental and numerical test results from previous studies to evaluate the effect of coarse particle shape. Fig. 7(a) shows that the Z_{CC}^m values in this study are greater than those of the previous spherical and ellipsoidal binary mixtures, especially at FC ≤ 60%. This finding may be due to the

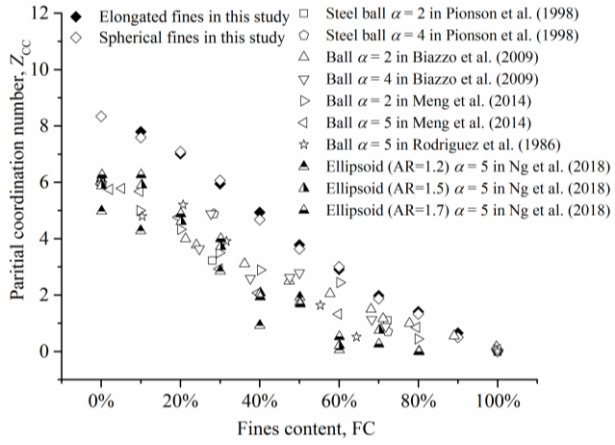

(a)

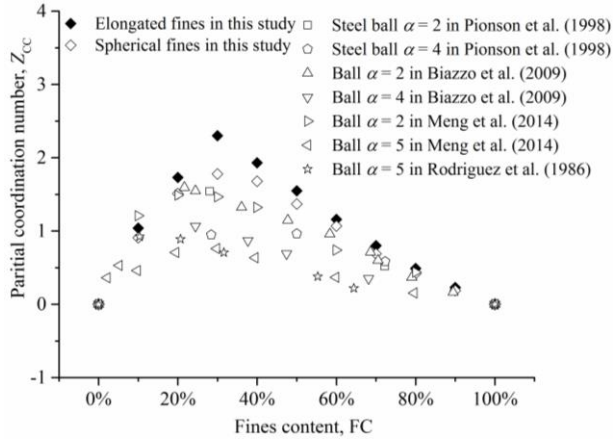

(b)

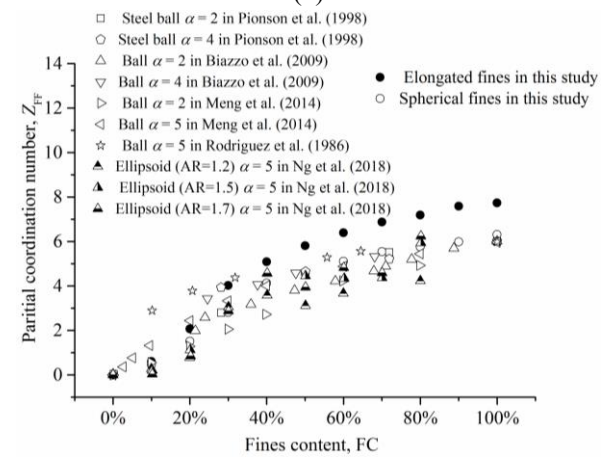

(c)

Fig. 7 Comparison of partial coordination numbers with other studies: (a) Z_{CC}^m; (b) Z_{CF}^m; (c) Z_{FF}^m

geometrical characteristic of the realistic gravel-shaped coarse particles used in our simulations. This observation is physically controlled by the following aspect: the surface areas of the gravel-shaped coarse particles are always larger than those of spherical particles with the same volume. This results in a greater probability for the gravel-shaped coarse particles to come into contact with each other, thus leading to a greater Z_{CC}^m. When FC > 60%, the coarse particles almost float in a matrix of fines, and there is only a small number of CC contacts, as indicated in Table 2. Therefore,

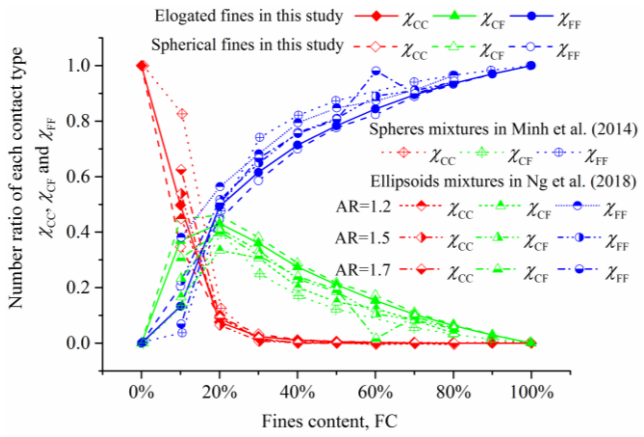

Fig. 8 Variation in the ratio of each contact type versus FC, with other DEM results for comparison

the particle shape of the coarse particles has only a small effect on Z_{CC}^{m} when FC > 60%. In addition, when compared to spherical coarse particles, the larger surface area of the gravel-shaped coarse particles also leads to more CF contacts. Consequently, Fig. 7(b) indicates slightly greater Z_{CF}^{m} values in this study. However, Fig. 7(c) shows that the Z_{FF}^{m} values in this study are generally consistent with the Z_{FF}^{m} values in other studies, indicating that the particle shape of coarse particles has an insignificant effect on Z_{FF}^{m}. Note that the Z_{FF}^{m} values of the elongated fines (AR = 1.5) are greater than those of the ellipsoid binary mixtures (AR = 1.2, 1.5 and 1.7) studied by Ng *et al*. (2018) because the frictionless condition used in this study produced the densest possible samples, whereas $\mu = 0.5$ was used in Ng *et al*. (2018) and loose samples were produced.

Another approach to study the contribution of the partial particle contacts is to analyze the ratios of the number of each contact type (χ_{CC}, χ_{CF} and χ_{FF}, as listed in Table 3). Fig. 8 illustrates the evolution of χ_{CC}, χ_{CF} and χ_{FF} versus FC; for comparison, the results of the 3D DEM simulations of dense binary mixtures consisting of spheres in Minh *et al*. (2014) and loose binary mixtures consisting of ellipsoids with different ARs in Ng *et al*. (2018) are also included. The general trends of χ_{CC}, χ_{CF} and χ_{FF} are consistent with the partial coordination numbers, as shown in Fig. 6. Referring to the results in this study, the effect of the particle shape of fines has only a small influence on χ_{CC}, χ_{CF} and χ_{FF}, except when FC = 10%. Therefore, although the particle shape of the fines influences the contact number of the CF and FF contacts, as shown in Table 2, it does not affect the distribution of the CF and FF contacts in the samples. At a given FC, differences in χ_{CC}, χ_{CF} and χ_{FF} are found in this study and other studies, indicating that the effects of the coarse particle shape and initial state (i.e., dense or loose) influence the distribution of each contact type in a binary mixture.

4. Shear characteristics

4.1 Macroscopic variable definitions

The dense isotropic samples were then numerically subjected to conventional drained triaxial compression tests by the downward displacement of the top wall at a constant velocity, whereas a constant confining pressure, enforced by the servo-control mechanism, acted on the lateral walls. For triaxial compression, a cylindrical soil sample is preferred. Considering the simple operability on the numerical triaxial compression tests, our numerical samples are cubic, which is similar with the true triaxial configuration and used in previous DEM studies (e.g., Antony and Kruyt, 2009, Gong and Liu 2017b). The macroscale stress tensor for the microscale quantities of the contact forces and contact vectors is as follows (Christoffersen *et al*. 1981):

$$\sigma_{ij} = \frac{1}{V}\sum_{c\in N_c} f_i^c d_j^c \tag{3}$$

where V is the total volume of the sample, N_c is the total number of contacts, f_i^c is the i*th* component of the contact force at contact c, and d_j^c is the j*th* component of the contact vector at contact c. Based on Eq. 3, the mean (p) and deviator (q) stresses commonly used in soil mechanics can be derived as follows

$$p = \frac{\sigma_1 + \sigma_2 + \sigma_3}{3}, \qquad q = \sigma_1 - \frac{\sigma_2 + \sigma_3}{2} \tag{4}$$

where σ_1 denotes the axial stress and σ_2 and σ_3 represent the lateral stresses. The axial strain ε_1 and the volumetric strain ε_v are derived from the movements of the rigid walls:

$$\varepsilon_1 = \frac{h_0 - h}{h_0}, \varepsilon_v = \frac{v_0 - v}{v_0} \tag{5}$$

where h_0 is the initial height of the assembly and h is the height at a given deformation; v_0 is the initial volume of the assembly and v is the volume of the assembly at the same given deformation state. Volumetric dilatancy is taken as negative in this study. The internal angle of friction, ϕ, which represents the shear strength of the granular material, can be defined from the stress ratio of a drained triaxial load based on the Mohr-Coulomb criterion:

$$sin\varphi = \frac{\sigma_1 - \sigma_3}{\sigma_1 + \sigma_3} = \frac{3q/p}{q/p + 6} \tag{6}$$

To ensure quasistatic shearing, the shear rate should be slow enough such that the kinetic energy generated during shearing can be considered negligible. This factor can be formulated in terms of an inertia parameter I, which was defined by Da Cruz *et al*. (2005):

$$I = \frac{\dot{\varepsilon}\bar{D}}{\sqrt{p/\rho}} \tag{7}$$

where $\dot{\varepsilon}$ is the axial compression strain rate and $\bar{D}$ is the mean diameter. Quasistatic shear in the granular system was ensured by a small I value. Agnolin *et al*. (2008) recommended that I remains below 1.0×10^{-3}, while Perez *et al*. (2016) recommended that it remains below 2.5×10^{-3}. The value of I was below 1.0×10^{-4} throughout the tests in this study.

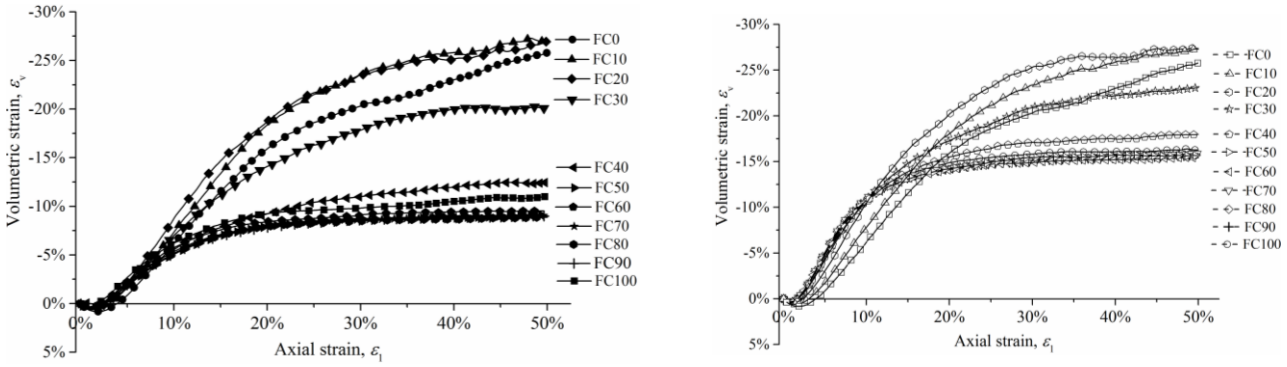

(a) (b)

Fig. 9 Evolution of ε_v with ε_1 for the two types of mixtures with different FCs: (a) spherical fines; (b) elongated fines

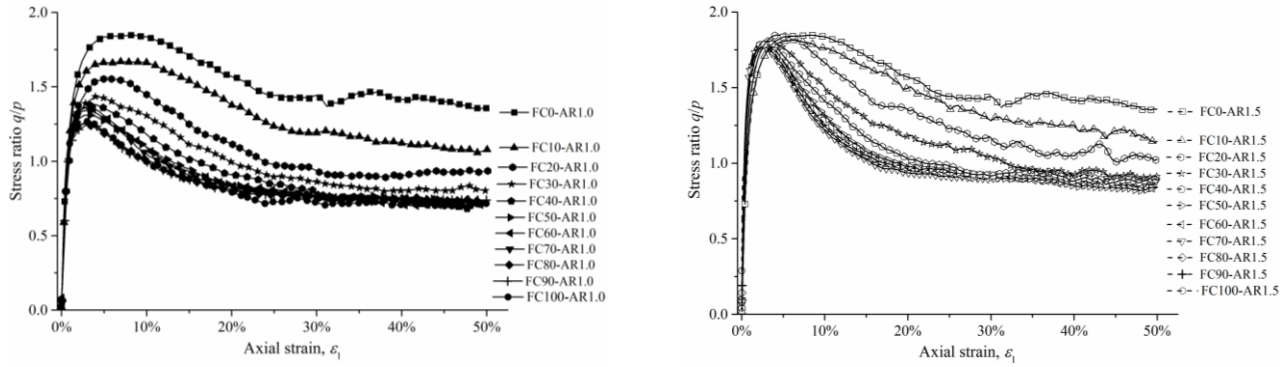

(a) (b)

Fig. 10 Evolution of q/p with ε_1 for the two types of mixtures with different FCs: (a) spherical fines; (b) elongated fines

4.2 Shear strength of the mixtures

To study the macroscopic and microscopic behaviors in the critical state, all samples were sheared to approximately 50% of ε_1. Figs. 9(a) and (b) illustrate the volumetric strain ε_v against the axial strain ε_1 for mixtures with spherical and elongated fines, respectively. Analogously, Figs. 10(a) and (b) present the stress ratio q/p versus ε_1 for the mixtures with different fines. As we can observe, the characteristic critical state conditions, i.e., a constant void ratio and stress ratio, are approximately satisfied at ε_1=50%. For the shear strength of mixtures as shown in Figs. 10(a)-(b), all curves exhibit a stiff response at the beginning of shear, and the q/p values reach a peak at a small axial strain. Then, the q/p values gradually decrease until eventually they approach the critical shear strength. The effects of the fine particle shape and content on the peak friction angle (φ_p) and the critical friction angle (φ_c) are depicted in Fig. 11. For spherical fines, the evolutions of φ_p and φ_c with FC are roughly consistent. Both φ_p and φ_c first decrease with an increase in FC when FC ≤ 30%~40% and then stabilize, with small fluctuations when FC > 30%~40%. A similar evolution of φ_p with FC was also found by Lu *et al*. (2017), who conducted biaxial compression tests of binary mixtures with polygonal coarse and discoid fine particles. For the mixtures with elongated fines, the evolutions of φ_p and φ_c with FC exhibit a different trend. Specifically, the φ_c value of the mixtures with elongated fines presents a similar evolution of the φ_p and φ_c values of the mixtures with spherical fines, while the corresponding φ_p value remains nearly unchanged with increasing FC. This observation suggests that for different fine particle shapes, the evolutions of φ_c and φ_p with FC depend on the relative magnitude of the friction angles of the pure coarse and fine materials. Specifically, when the friction angles of the coarse and fine materials become more similar, FC has a small effect on altering the friction angles of the granular mixtures. This relationship was observed by Chang *et al*. (2016), who studied the shear resistance of gravelly soils through a series of drained simple shear tests. However, when there is a marked difference between the friction angles of the coarse and fine materials, the evolutions of the friction angles with FC follow a specific pattern. Specifically, when FC ≤ 30%~40%, φ_c and φ_p gradually decrease with increasing FC. This result could be because the granular mixtures are coarse-dominated materials, and a continuous increase in FC weakens the interlocking effect among the coarse particles. However, when FC > 30%~40%, the φ_p and φ_c values are almost invariant, which is possible because most of the coarse particles are surrounded by fines. In this case, there are only a few coarse particles in contact each other, and the contact forces are transmitted among CF contacts or merely among FF contacts. A further increase in FC thus has a small effect on the shear strength of a granular mixture. Therefore, in our simulations, FC = 30%~40% indicates a transition in which the granular mixture changes from a coarse-dominated material to a coarse-fine-interaction material. Notably, this FC threshold agrees with the FC at which the binary

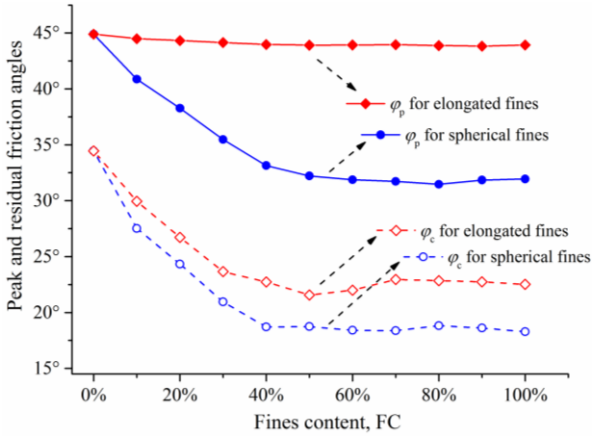

Fig. 11 Variations in φ_p and φ_c of the two types of mixtures with respect to FC

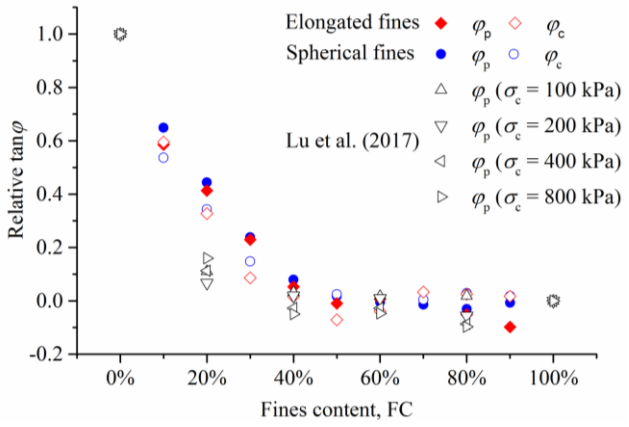

Fig. 12 The trends for relative tanφ plotted against FC

mixtures reach a minimum porosity (i.e., FC ≈ 30%, as observed in Fig. 4). Previous experimental studies also determined that this threshold (i.e., FC = 30%~40%) is usually a critical turning point of the shear strength of granular mixtures (e.g., Kuenza *et al*. 2004, Vallejo 2001) and the liquefaction resistance of silt and sand mixtures (e.g., Polito *et al*. 2001, Thevanayagam *et al*. 2002, Yang *et al*. 2006). As we can observe in Fig. 11, when FC > 40%, φ_c values are about 18° and 23° for the mixtures with spherical fines and elongated fines, respectively. Bolton (1986) organized the φ_c values of different sands from many literatures and found that the φ_c values of those sand ranged from 30° to 37°. Obviously, the φ_c values in this study are much smaller than the actual granular materials. This finding can be attributed to the particle shape effect. Specifically, the spherical and elongated fines in this study are deviated from the actual particle shape, which cause less interlock effect and thus have a smaller φ_c values.

Fig. 12 illustrates the trends of the relative tanφ plotted against FC. The relative tanφ = (tanφ_i-tanφ_{iF})/(tanφ_{iC}-tanφ_{iF}), where tanφ_i denotes either tanφ_p or tanφ_c and tanφ_{iF} and tanφ_{iC} indicate the friction angles of the models with pure fine particles (i.e., FC100) and pure coarse particles (i.e., FC0), respectively. For comparison, the relative tanφ of the peak friction angles for different σ_c values presented by Lu *et al*. (2017) (DEM simulations on binary mixtures of polygonal coarse and discoid fine particles) are included in Fig. 12. All the relative tanφ values gradually decrease from 1.0 to 0.0 when FC increases from 0% to 30%~40%. When FC ≥ 30%~40%, all the relative tanφ values approach zero with only small fluctuations. The trend of relative tanφ also characterizes the transition from a coarse-dominated material to a coarse-fine-interaction material at FC = 30%~40%. Comparing the values of φ (Fig. 11) and the relative tanφ (Fig. 12) from this study, the effect of the fine particle shape is not represented when using the relative tanφ. Namely, the fine particle shape influences the magnitudes of φ_p and φ_c but does not affect the evolution trend of the relative tanφ. When compared to the relative tanφ presented by Lu *et al*. (2017), greater relative tanφ values are observed at FC = 20% in this study, possibly due to the effect of the particle shape of the coarse particles. That is, realistic gravel-shaped coarse particles were used in this study, whereas polygonal coarse particles were adopted in the study of Lu *et al*. (2017).

4.3 Anisotropies of origins of strength

The packing and shear characteristics mentioned above provide a basic picture of the effects of the content and particle shape of fines. However, this picture is insufficient since the contact and force networks are generically anisotropic. Figs. 13(a)-(c) present snapshots of the contact force networks for the sample FC20-AR1.5 during deformation: (a) at the initial state; (b) at the peak state; and (c) at the critical state. In Fig. 13, the line thickness is proportional to the contact force. This figure shows that the contact forces are generally isotropic at the initial state. However, the large contact forces have a preferential vertical orientation (i.e., they are preferentially aligned with the major principal stress direction) at the peak and critical states. In this section, the fabric anisotropies are analyzed to understand the origins of the macroscale shear strengths, emphasizing the evaluation of the anisotropies and the relation between the anisotropies and the origins of the peak and residual shear strengths. Note that no shear banding localization and the small contact forces near the model boundaries has been observed in Fig. 13. These findings are most likely because the study uses rigid boundary walls, which will inhibit natural development of localization and the stress distribution along the boundaries as reported in Cheung and O'Sullivan (2008).

The anisotropies of the contact normal and contact forces play an important role in the shear behavior of granular material (Gu *et al*. 2014, Guo and Zhao 2013). The distribution of the contact normal can be described by the fabric tensor as follows (Satake 1982)

$$\Phi_{ij} = \int_{\Omega} E(\Omega) n_i n_j d\Omega = \frac{1}{N} \sum_{c \epsilon N_c} n_i n_j \tag{8}$$

where n_i is the unit contact normal vector in the i direction and Ω denotes the orientation of the contact normal in spherical coordinates. $E(\Omega)$ is the distribution probability

function and can be expressed as follows:

$$E(\Omega) = \frac{1}{4\pi}[1 + a_{ij}^{\mathrm{c}} n_i n_j\ ] \tag{9}$$

where a_{ij}^{c} is the second-order anisotropy tensor, which is deviatoric and symmetric and used to characterize the fabric anisotropy. a_{ij}^{c} can be determined from the deviatoric part of the fabric tensor Φ_{ij}'.

$$a_{ij}^{\mathrm{c}} = \frac{15}{2}\Phi_{ij}' \tag{10}$$

With respect to the direction of the contact normal, the contact force can be split into normal and tangential components: F_{ij}^{n} and F_{ij}^{t}, given in Eqs. 11 and 13 (Guo and Zhao 2013, Rothenburg *et al*. 1989).

$$F_{ij}^{\mathrm{n}} = \frac{\int_{\Omega} \bar{f}^{\mathrm{n}}(\Omega) n_i n_j d\Omega}{4\pi} = \sum_{1}^{N_{\mathrm{c}}} \frac{f_{\mathrm{n}} n_i n_j}{N_{\mathrm{c}}[1 + a_{kl}^{\mathrm{c}} n_k n_l]} \tag{11}$$

$$\overline{f}^{\mathrm{n}}(\Omega) = \bar{f}_0\left(1 + a_{ij}^{\mathrm{n}} n_i n_j\ \right) \tag{12}$$

$$F_{ij}^{\mathrm{t}} = \frac{\int_{\Omega} \bar{f}^{\mathrm{t}}(\Omega) t_i n_j d\Omega}{4\pi} = \sum_{1}^{N_{\mathrm{c}}} \frac{f_{\mathrm{t}} t_i n_j}{N_{\mathrm{c}}[1 + a_{kl}^{\mathrm{c}} n_k n_l]} \tag{13}$$

$$\bar{f}^{\mathrm{t}}(\Omega) = \bar{f}_0\left(a_{ij}^{\mathrm{t}} n_j\ - (a_{kl}^{\mathrm{t}} n_k n_l\ ) n_i\ \right) \tag{14}$$

Eqs. 12 and 14 represent the probability distributions of F_{ij}^{n} and F_{ij}^{t}, respectively, where

$$a_{ij}^{\mathrm{n}} = \frac{15F_{ij}^{\mathrm{n}\prime}}{2\bar{f}_0} \qquad a_{ij}^{\mathrm{t}} = \frac{5F_{ij}^{\mathrm{t}\prime}}{\bar{f}_0} \tag{15}$$

and $F_{ij}^{\mathrm{n}\prime}$ and $F_{ij}^{\mathrm{t}\prime}$ are the deviatoric parts of F_{ij}^{n} and F_{ij}^{t}, respectively. $\bar{f}_0$=F_{ii}^{n} is the average normal contact force calculated based on the entire range of Ω and is different from the mean normal contact force averaged over all of the contacts. Clearly, the branch vector length can be expressed similarly to the form of the normal and tangential contact forces. By replacing the normal and tangential contact force to the length of the branch vector in Eqs. 11 and 13, one obtains:

$$a_{ij}^{\mathrm{bn}} = \frac{15B_{ij}^{\mathrm{n}\prime}}{2\overline{d_0}} \qquad a_{ij}^{\mathrm{bt}} = \frac{5B_{ij}^{\mathrm{t}\prime}}{\overline{d_0}} \tag{16}$$

Because the fabric tensor is deviatoric in nature, it is convenient to use a scalar a_* that is obtained from the invariants of each anisotropy tensor (namely, a_{ij}^{c}, a_{ij}^{n}, a_{ij}^{t}, a_{ij}^{bn} and a_{ij}^{bt}) and that can reflect the degree of fabric anisotropy as follows:

$$a_* = \mathrm{sign}(\mathrm{S_r})\sqrt{\frac{3a_{ij}^* a_{ij}^*}{2}} \tag{17}$$

where a_* represents the anisotropic coefficients a_{c}, a_{n}, a_{t}, a_{bn} and a_{bt} corresponding to one of the five cases of anisotropy previously mentioned. S_{r} is a normalized quantity of the double contraction of a_{ij}^* and σ_{ij}^* and can be defined as follows (Guo and Zhao 2013):

$$\mathrm{S_r} = \frac{a_{ij}^* \sigma_{ij}^*}{\sqrt{a_{kl}^* a_{kl}^*}\sqrt{a_{mn}^* a_{mn}^*}} \tag{18}$$

Guo and Zhao (2013) derived the following relationship between the stress-force-fabric and the stress ratio

$$\frac{q}{p} = 0.4(a_{\mathrm{c}} + a_{\mathrm{n}} + 1.5a_{\mathrm{t}} + a_{\mathrm{bn}} + 1.5a_{\mathrm{bt}}) \tag{19}$$

Note that the cross products of the two anisotropic tensors are neglected in the right-hand term of Eq. 19. In addition, Eq. 19 is obtained under the assumption that the contact forces and the branch vectors in the granular system are uncorrelated. However, previous numerical studies have demonstrated that the CC contacts in binary mixtures often capture the largest contact forces, followed by the CF and FF contacts (Gong *et al*. 2019a, Voivret *et al*. 2009). In other words, the contact forces are dependent on the length of the branch vectors. Therefore, the assumption of uncorrelated contact forces and branch vectors may not be fulfilled for binary mixtures. The effectiveness of the stress-force-fabric relationship given in Eq. 19 needs verification.

To validate Eq. 19, q/p obtained from the DEM data is compared with that from the anisotropies, as indicated in Figs. 14(a)-(c). Fig. 14(a) shows the contribution of each anisotropy coefficient to the macroscopic q/p for FC50-AR1.5. Figs. 14(b) and (c) illustrate the variations in q/p with FC for the models with spherical and elongated fines at the peak and critical states, respectively, with the analytical expression given by Eq. 19. In Fig. 14(a), q/p compares well with the stress-force-fabric relationship given in Eq. 19, even though the analytical expression slightly underestimates q/p before the critical state. Similar observations are also shown in Figs. 14(b) and (c); for various samples, Eq. 19 underestimates q/p at the peak state but provides a better fit at the critical state. The underestimation may be attributed to the fact that Eq. 19 neglects the cross products of the two anisotropic tensors and assumes that the contact forces and branch vectors are uncorrelated. Although Eq. 19 underestimates the peak q/p, Figs. 14(b) and (c) show that the evolutions of q/p at the peak and critical states obtained from Eq. 19 are generally consistent with those obtained from the DEM data. Therefore, the anisotropies defined in Eq. 17 are generally reasonable. The stress-force-fabric relationship connects the shear strength of granular materials and their anisotropies and provides a way to quantify the role of each anisotropy coefficient that contributes to the shear strength. For example, Fig. 14(a) shows that a_{n} provides the greatest contribution to the shear strength, followed by a_{c} and a_{t}, which together dominantly determine the shear strength, while the contributions of a_{bn} and a_{bt} to the shear strength can be neglected.

The emphasis of anisotropic analysis is placed on evaluating the anisotropy cofficients a_{c}, a_{n} and a_{t}. The anisotropy cofficients a_{bn} and a_{bt} are not of concern here because of their insignificant contribution to the shear strength. The evolutions of anisotropies a_{c}, a_{n} and a_{t} with FC are displayed in Fig. 15 for the two types of mixtures at the critical state. The evolutions of anisotropy coefficients

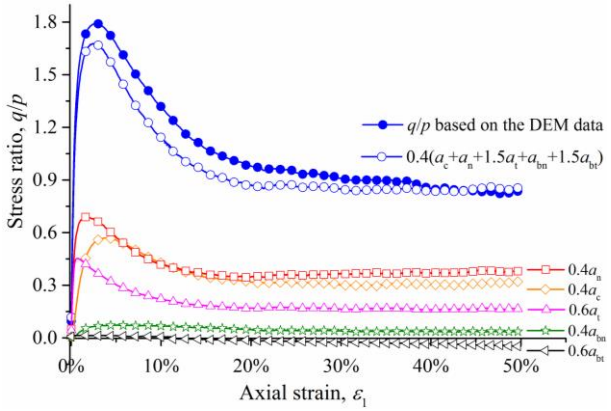

(a)

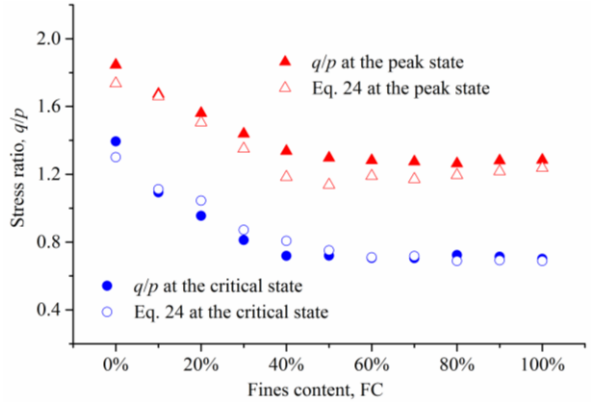

(b)

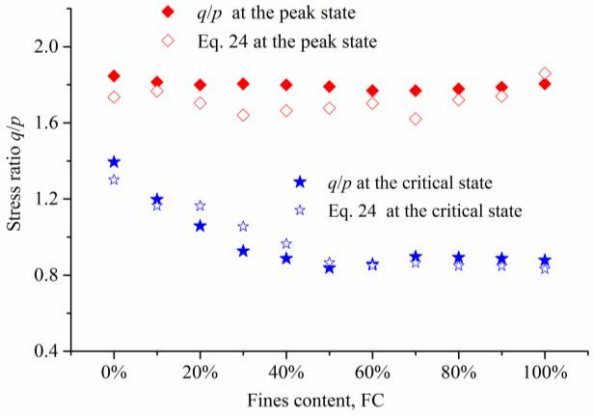

(c)

Fig. 14 Validation of the stress-force-fabric relationship: (a) evolution of q/p and the anisotropies for FC20-AR1.5 with 1; (b) variation in peak and critical q/p with FC for the spherical fines with the analytical expression given in Eq. 24; (c) variation in peak and critical q/p with FC for the elongated fines with the analytical expression given in Eq. 24

a_c, a_n and a_t for these mixtures exhibit a similar trend. Specifically, both a_c and a_t first gradually decrease with increasing FC and then plateau when FC $\geq$ 40%. However, a_n shows a unimodal pattern, namely, a_n initially increases as FC increases, reaches a peak value at FC $\approx$ 40%, then slightly decreases and eventually plateaus when FC $\geq$ 60%. Note that the above features are also observed at the peak state but are not shown here. For a given FC, the

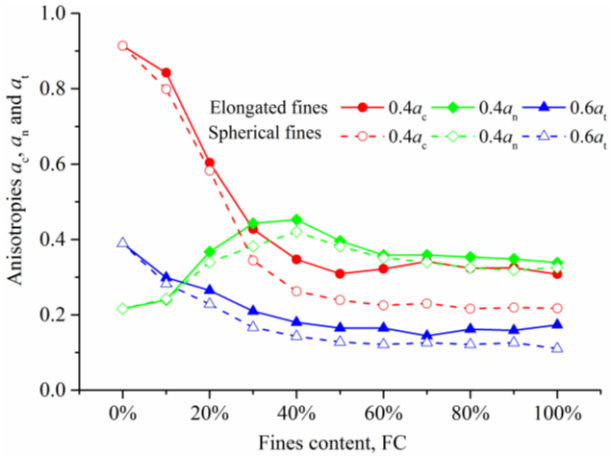

Fig. 15 Validation in the anisotropies (i.e., a_c, a_n and a_t) at the critical states with FC for two types of fines

anisotropy coefficients a_c, a_n and a_t of the elongated fines are greater than those of the spherical fines. This result agrees well with previous numerical simulations that investigated the shear strength of pure elongated particles (Azema *et al*. 2010b). Based on the anisotropic analysis, the shear strength of binary mixtures is clearly a joint effect of a_c, a_n and a_t. At FC $\leq$ 40%, the decrease in φ_c (as shown in Fig. 11) primarily depends on the decrease in a_c and a_t, which is markedly more significant than the increase in a_n. The same anisotropic mechanism is also applied to explain the decrease in φ_p of the spherical fines. Nevertheless, the stabilization of φ_p of the elongated fines (as shown in Fig. 11) is due to the decrease in a_c and a_t to compensate the increase in a_n. At FC > 40%, both a_c and a_t remain nearly unchanged; however, a_n slightly decreases when FC increases from 40% to 60% and then remain constant when FC $\geq$ 60%. Therefore, both φ_c and φ_p remain approximately stable when FC > 40% (as shown in Fig. 11).

5. Conclusions

The packing and shear characteristics of binary mixtures were studied using a 3D DEM. The binary mixtures consisted of realistic gravel-shaped coarse particles and fine particles with one of two shapes. The fine particle shapes evaluated were spherical and elongated, which can be represented by their AR values (1.0 and 1.5). The macroscopic and microscopic packing and shear characteristics of the packed binary mixtures were examined. The main conclusions are summarized below.

For both spherical and elongated fines, e_0 first decreases and then increases as FC continuously increases. However, e_0 of the spherical fines is greater than that of the elongated fines, which is due to the space-filling effect as the AR of the particles increases. For fines with elongated particles, greater overall (Z_o) and mechanical (Z_m) coordination numbers values are observed for spherical fines, possibly due to the lower initial void ratios that originate from the space-filling effect. The evolutions of three types of partial coordination number (i.e., Z_{CC}^{m}, Z_{CF}^{m} and Z_{FF}^{m}) with FC are similar between the models that use the two fine shapes.

When comparing the results of this study with those of other studies on spherical binary mixtures, greater Z_{CC}^{m} and Z_{CF}^{m} and similar Z_{FF}^{m} values are observed in this study, attributed to the different geometrical characteristics of the coarse particles. The particle shape of the fines affects the total number of CF and FF contacts but not the distributions of the numbers of each contact type.

The effects of the particle shape and FC on the peak and critical friction angles of binary mixtures were examined. φ_p and φ_c of the spherical fines and φ_c of the elongated fines gradually decrease with increasing FC when FC ≤ 30%~40% and are almost invariant when FC > 30%~40%. However, the φ_p value of the elongated fines remains nearly unchanged with increasing FC. Therefore, for different fine particle shapes, the evolutions of φ_c and φ_p of binary mixtures with a nonzero FC depend on the relative magnitude of the friction angles of the pure coarse and fine materials. The effect of fine particle shape on the friction angles of binary mixtures is not captured by the relative tanφ-FC relationship. The relation between the anisotropies and the origins of the peak and critical shear strengths were evaluated. The shear strengths of binary mixtures are mainly controlled by the anisotropy coefficients a_c, a_n and a_t and are less affected by the anisotropy coefficients a_{bn} and a_{bt}. The evolutions of a_c, a_n and a_t of the two types of fines exhibit similar trends. The shear strengths of binary mixtures are a joint effect of a_c, a_n and a_t, allowing us to highlight the anisotropic mechanism that leads to the dependence of shear strength on the particle shape and FC.

Acknowledgments

This research is supported by the National Natural Science Foundation of China (No. 51809292, 51478481 and 51878668), Postdoctoral Fund of Central South University (No. 205455) and Beijing Municipal Science and Technology Project: Research and Application of Design and Construction Technology of Railway Engineering Traveling the Rift Valley (No. Z181100003918005). The authors would like to express their appreciation to the financial assistance.

References

Abbireddy, C.O.R. and Clayton, C.R.I. (2010), "Varying initial void ratios for DEM simulations", *Geotechnique*, **60**(6), 497-502. https://doi.org/10.1680/geot.2010.60.6.497.

Agnolin, I. and Roux, J.N. (2008), "On the elastic moduli of three-dimension assemblies of spheres: Characterization and modeling of fluctuations in the particle displacement and rotation", *Int. J. Solids Struct.*, **3**(45), 1101-1123. https://doi.org/10.1016/j.ijsolstr.2007.07.016.

Antony S J, Kruyt N P. (2009), "Role of interparticle friction and particle-scale elasticity in the shear-strength mechanism of three-dimensional granular media", *Phys. Rev. E.*, **79**, 031308. https://doi.org/10.1103/PhysRevE.79.031308.

Azema, E. and Radjai, F. (2010a), "Stress-strain behavior and geometrical properties of packings of elongated particles", *Phys. Rev. E.*, **81**, 05130451. https://doi.org/10.1103/PhysRevE.81.051304.

Azema, E., Preechawuttipong, I. and Radjai, F. (2016a), "Binary mixtures of disks and elongated particles: texture and mechanical properties", *Phys. Rev. E.*, **94**, 0429014. https://doi.org/10.1103/PhysRevE.94.042901.

Berger, K.J. and Hrenya, C.M. (2014), "Challenges of DEM: ii. Wide particle size distributions", *Powder Technol.*, **264**, 627-633. https://doi.org/10.1016/j.powtec.2014.04.096.

Biazzo, I., Caltagirone, F., Parisi, G. and Zamponi, F. (2009), "Theory of amorphous packings of binary mixtures of hard spheres", *Phys. Rev. Lett.*, **102**, 19570119. https://doi.org/10.1103/PhysRevLett.102.195701.

Bolton, M.D. (1986), "The strength and dilatancy of sands", *Geotechnique*, **36**(1), 65-78. https://doi.org/10.1680/geot.1986.36.1.65.

Chang, W. and Phantachang, T. (2016), "Effects of gravel content on shear resistance of gravelly soils", *Eng. Geol.*, **207**, 78-90. https://doi.org/10.1016/j.enggeo.2016.04.015.

Cheung, G. and O'Sullivan, C. (2008), "Effective simulation of flexible lateral boundaries in two- and three-dimensional DEM simulations", *Particuology*, **6**, 483-500. https://doi.org/10.1016/j.partic.2008.07.018.

Christoffersen, J., Mehrabadi, M.M. and Nemat-Nasser, S. (1981), "A micromechanical description of granular material behavior", *Transactions ASME J. Appl. Mech.*, **48**(2), 339-344. https://doi.org/10.1115/1.3157619.

Cundall, P.A. and Strack, O.D.L. (1979), "A discrete numerical model for granular assemblies", *Geotechnique*, **29**, 47-65. https://doi.org/10.1680/geot.1979.29.1.47.

Da Cruz, F., Emam, S., Prochnow, M., Roux, J.N. and Chevoir, F. (2005), "Rheophysics of dense granular materials: discrete simulation of plane shear flows", *Phys. Rev. E.*, **72**, 02130921. https://doi.org/10.1103/PhysRevE.72.021309.

Dai BB, Yang J, Gu XQ, Zhang Wei. (2019), "A numerical analysis of the equivalent skeleton void ratio for silty sand", *Geomech. Eng.*, **17**(1), 19-30. https://doi.org/10.12989/gae.2019.17.1.019.

Dai, BB and Yang, J. (2017), "Shear strength of assemblies of frictionless particles", *Int. J. Geomech.*, **17**, 0401710211. https://doi.org/10.1061/(ASCE)GM.1943-5622.0001005.

Dai, BB, Yang, J. and Luo, X. (2015), "A numerical analysis of the shear behavior of granular soil with fines", *Particuology*, **21**, 160-172. https://doi.org/10.1016/j.partic.2014.08.010.

Dai, BB., Yang, J. and Zhou, C.Y. (2016), "Observed effects of interparticle friction and particle size on shear behavior of granular materials", *Int. J. Geomech.*, **16**, 040150111. https://doi.org/10.1061/(ASCE)GM.1943-5622.0000520.

De Frias Lopez, R., Ekblad, J. and Silfwerbrand, J. (2016), "Resilient properties of binary granular mixtures: A numerical investigation", *Comput. Geotech.*, **76**, 222-233. https://doi.org/10.1016/j.compgeo.2016.03.002.

De Frias Lopez, R., Silfwerbrand, J., Jelagin, D. and Birgisson, B. (2016), "Force transmission and soil fabric of binary granular mixturese", *Geotechnique*, **66**(7), 578-583. https://doi.org/10.1680/jgeot.14.P.199.

Goldenberg, C. and Goldhirsch, I. (2005), "Friction enhances elasticity in granular solids", *Nature*, **435**(7039), 188-191. https://doi.org/10.1038/nature03497.

Gong, J, Zou J F, Zhao L H, Nie Z H. (2019b), "New insights into the effect of interparticle friction on the critical state friction angle of granular materials", *Comput. Geotech.*, **113**, 103105. https://doi.org/10.1016/j.compgeo.2019.103105.

Gong, J. and Liu, J. (2017a), "Analysis of the thresholds of granular mixtures using the discrete element method", *Geomech. Eng.*, **12**(4), 639-655. https://doi.org/10.12989/gae.2017.12.4.639.

Gong, J. and Liu, J. (2017b), "Effect of aspect ratio on triaxial compression of multisphere ellipsoid assemblies simulated

using a discrete element method", *Particuology*, **32**, 49-62. https://doi.org/10.1016/j.partic.2016.07.007.

Gong, J., Nie Z H, Zhu Y G, Liang Z Y, Wang X. (2019a), "Exploring the effects of particle shape and content of fines on the shear behavior of sand-fines mixtures via the DEM", *Comput. Geotech.*, **106**, 161-176. https://doi.org/10.1016/j.compgeo.2018.10.021.

Gu, XQ, Hu, J. and Huang, M. (2017), "Anisotropy of elasticity and fabric of granular soils", *Granul. Matter*, **19**(2), 33. https://doi.org/10.1007/s10035-017-0717-6.

Gu, XQ, Hu, J., Huang, M. and Yang, J. (2018), "Discrete element analysis of the k-0 of granular soil and its relation to small strain shear stiffness", *Int. J. Geomech.*, **18**, 060180033. https://doi.org/10.1061/(ASCE)GM.1943-5622.0001102.

Gu, XQ, Huang, M. and Qian, J. (2014), "DEM investigation on the evolution of microstructure in granular soils under shearing", *Granul. Matter*, **16**(1), 91-106. https://doi.org/10.1007/s10035-013-0467-z.

Gu, XQ, Zhang JQ, Huang X. (2020), "DEM analysis of monotonic and cyclic behaviors of sand based on critical state soil mechanics framework", *Comput. Geotech.*, **128**, 103787. https://doi.org/10.1016/j.compgeo.2020.103787.

Guarin, A., Roque, R., Kim, S. and Sirin, O. (2013), "Disruption factor of asphalt mixtures", *Int. J. Pavement Eng.*, **14**(5), 472-485. https://doi.org/10.1080/10298436.2012.727992.

Guo, N. and Zhao, J. (2013), "The signature of shear-induced anisotropy in granular media", *Comput. Geotech.*, **47**, 1-15. https://doi.org/10.1016/j.compgeo.2012.07.002.

Hall, S.A., Bornert, M., Desrues, J., Pannier, Y., Lenoir, N., Viggiani, G. and Besuelle, P. (2010), "Discrete and continuum analysis of localised deformation in sand using x-ray mu ct and volumetric digital image correlation", *Geotechnique*, **60**(5), 315-322. https://doi.org/10.1680/geot.2010.60.5.315.

Harehdasht, S.A., Karray, M., Hussien, M.N. and Chekired, M. (2017), "Influence of particle size and gradation on the stress-dilatancy behavior of granular materials during drained triaxial compression", *Int. J. Geomech.*, **17**, 040170779. https://doi.org/10.1061/(ASCE)GM.1943-5622.0000951.

Itasca (2014), User's manual for pfc3d; Itasca consulting Group Inc.; Minneapolis, USA

Jamiolkowski, M., Kongsukprasert, L. and Lo Presti, D. (2004), "Characterization of gravelly geomaterials", *Proceedings of The Fifth International Geotechnical Conference*, Bangkok, Thailand, November.

Krishna, P. and Pandey, D. (1981), "Close-packed structures", *International Union of Crystallography Commission on Crystallographic Teaching, First Series Pamphlets, No 5*., University College Cardiff Press, Cardiff, 1981.

Kristiansen, K.D., Wouterse, A. and Philipse, A. (2005), "Simulation of random packing of binary sphere mixtures by mechanical contraction", *Physica A*, **358**(2-4), 249-262. https://doi.org/10.1016/j.physa.2005.03.057.

Kuenza, K., Towhata, I., Orense, R.P. and Wassan, T.H. (2004), "Undrained torsional shear tests on gravelly soils", *Landslides*, **1**(3), 185-194. https://doi.org/10.1007/s10346-004-0023-3.

Lade, P.V., Liggio, C.D. and Yamamuro, J.A. (1998), "Effects of non-plastic fines on minimum and maximum void ratios of sand", *Geotech. Test J.*, **21**(4), 336-347. https://doi.org/10.1520/GTJ11373J.

Lu, Y., Tan, Y., Li, X. and Liu, C. (2017), "Methodology for simulation of irregularly shaped gravel grains and its application to DEM modeling", *J. Comput. Civil Eng.*, **3**, 040170235. https://doi.org/10.1061/(ASCE)CP.1943-5487.0000676.

Meng, L., Lu, P. and Li, S. (2014), "Packing properties of binary mixtures in disordered sphere systems", *Particuology*, **16**, 155-166. https://doi.org/10.1016/j.partic.2014.02.010.

Minh, N.H. and Cheng, Y.P. (2013), "A DEM investigation of the effect of particle-size distribution on one-dimensional compression", *Geotechnique*, **63**(1), 44-53. https://doi.org/10.1680/geot.10.P.058.

Minh, N.H., Cheng, Y.P. and Thornton, C. (2014), "Strong force networks in granular mixtures", *Granul Matter*, **16**(1), 69-78. https://doi.org/10.1007/s10035-013-0455-3.

Ng, T., Zhou, W. and Chang, X. (2017), "Effect of particle shape and fine content on the behavior of binary mixture", *J. Eng. Mech.*, **143**, C40160081SI. https://doi.org/10.1061/(ASCE)EM.1943-7889.0001070.

Ng, T., Zhou, W., Ma, G. and Chang, X. (2018), "Macroscopic and microscopic behaviors of binary mixtures of different particle shapes and particle sizes", *Int J Solids Struct*, **135**, 74-84. https://doi.org/10.1016/j.ijsolstr.2017.11.011.

Peng, Y. and Bao, J. (2018), "Comparative study of 2d and 3d micromechanical discrete element modeling of indirect tensile tests for asphalt mixtures", *Int. J. Geomech.*, **18**, 040180466. https://doi.org/10.1061/(ASCE)GM.1943-5622.0001155.

Perez, J.L., Kwork, C.Y., Huang, X. and Hanley, K.J. (2016), "Assessing the quasi-static conditions for shearing in granular media within the critical state soil mechanics framework", *Soils Found*, **1**(56), 152-159. https://doi.org/10.1016/j.sandf.2016.01.013.

Pinson, D., Zou, R.P., Yu, A.B., Zulli, P. and McCarthy, M.J. (1998), "Coordination number of binary mixtures of spheres", *J. Phys. D Appl. Phys.*, **31**, 457-462. https://doi.org/10.1088/0022-3727/31/4/016.

Polito, C.P. and Martin, J.R. (2001), "Effects of nonplastic fines on the liquefaction resistance of sands", *J. Geotech. Geoenviron.*, **127**(5), 408-415. https://doi.org/10.1061/(ASCE)1090-0241(2001)127:5(408).

Rodriguez, J., Allibert, C.H. and Chaix, J.M. (1986), "A computer method for random packing of spheres of unequal size", *Powder Technol.*, **47**(1), 25-33. https://doi.org/10.1016/0032-5910(86)80004-3.

Rothenburg, L. and Bathurst, R.J. (1989), "Analytical study of induced anisotropy in idealized granular materials", *Geotechnique*, **39**(4), 601-614. https://doi.org/10.1680/geot.1989.39.4.601.

Satake, M. (1982), "Fabric tensor in granular materials", *Deformation and Failure of Granular Materials*, *International Union of Theoretical and Applied Mechanics Symposium on Deformation and Failure of Granular Materials*, Delft, Netherlands, August-September. 63-68.

Shire, T. and O'Sullivan, C. (2013), "Micromechanical assessment of an internal stability criterion", *Acta Geotech.*, **8**(1), 81-90. https://doi.org/10.1007/s11440-012-0176-5.

Shire, T., O'Sullivan, C. and Hanley, K.J. (2016), "The influence of fines content and size-ratio on the micro-scale properties of dense bimodal materials", *Granul. Matter*, **18**(3), 1-10. https://doi.org/10.1007/s10035-016-0654-9.

Suzuki, M., Kada, H. and Hirota, M. (1999), "Effect of size distribution on the relation between coordination number and void fraction of spheres in a randomly packed bed", *Adv. Powder Technol.*, **10**(4), 353-365. https://doi.org/10.1163/156855299X00208.

Taghavi, R. (2011), "Automatic clump generation based on mid-surface", *Continuum and Distinct Element Modeling in Geomechanics*, *Proceedings of 2nd International FLAC/DEM Symposium*, Melbourne, February, 791-797.

Thevanayagam, S., Shenthan, T., Mohan, S. and Liang, J. (2002), "Undrained fragility of clean sands, silty sands and sandy silts", *J. Geotech. Geoenviron*, **128**(10), 849-859. https://doi.org/10.1061/(ASCE)1090-0241(2002)128:10(849).

Thornton, C. (2000), "Numerical simulations of deviatoric shear deformation of granular media", *Geotechnique*, **50**(1), 43-53. https://doi.org/10.1680/geot.2000.50.1.43.

Ueda, T., Matsushima, T. and Yamada, Y. (2011), "Effect of particle size ratio and volume fraction on shear strength of

binary granular mixture", *Granul. Matter*, **13**(6), 731-742. https://doi.org/10.1007/s10035-011-0292-1.
Vallejo, L.E. (2001), "Interpretation of the limits in shear strength in binary granular mixtures", *Can. Geotech. J.*, **38**(5), 1097-1104. https://doi.org/10.1139/t01-029.
Voivret, C., Radjai, F., Delenne, J.Y. and El Youssoufi, M.S. (2009), "Multiscale force networks in highly polydisperse granular media", *Phys. Rev. Lett.*, **102**, 17800117. https://doi.org/10.1103/PhysRevLett.102.178001/
Wang, J J., Qiu, ZF., Deng WJ. (2016), "Effects of mudstone particle content on shear strength of a crushed sandstone-mudstone particle mixture", *Marine Georesources Geotechnol.*, **34**(4), 395-402. https://doi.org/10.1080/1064119X.2014.961621.
Wang, JJ., Zhang, HP., Deng, DP. and Liu, MW. (2013), "Effects of mudstone particle content on compaction behavior and particle crushing of a crushed sandstone-mudstone particle mixture", *Eng. Geol.*, **167**, 1-5. https://doi.org/10.1016/j.enggeo.2013.10.004.
Wang, L., Park, J. and Fu, Y. (2007), "Representation of real particles for DEM simulation using x-ray tomography", *Constr. Build Mater.*, **21**(2), 338-346. https://doi.org/10.1016/j.conbuildmat.2005.08.013.
Wang, L., Park, J. and Fu, Y. (2007), "Representation of real particles for DEM simulation using X-ray tomography", *Constr. Build. Mater.*, **21**(2), 338-346. https://doi.org/10.1016/j.conbuildmat.2005.08.013.
Weatman, A.E.R. (1936), "The packing of particles: Empirical equation for intermediate diameter ratios", *J. Americal Ceramic Soc.*, **19**(1-12), 127-129. https://doi.org/10.1111/j.1151-2916.1936.tb19809.x.
Wei, H., Xu, W., Xu, X., Meng, Q. and Wei, C. (2018), "Mechanical properties of strongly weathered rock-soil mixtures with different rock block contents", *Int. J. Geomech.*, **18**, 040180265. https://doi.org/10.1061/(ASCE)GM.1943-5622.0001131.
Xu, W., Hu, L. and Gao, W. (2016), "Random generation of the meso-structure of a soil-rock mixture and its application in the study of the mechanical behavior in a landslide dam", *Int. J. Rock Mech. Min.*, **86**, 166-178. https://doi.org/10.1016/j.ijrmms.2016.04.007.
Xu, W., Xu, Q. and Hu, R. (2011), "Study on the shear strength of soil-rock mixture by large scale direct shear test", *Int. J. Rock Mech. Min.*, **48**(8), 1235-1247. https://doi.org/10.1016/j.ijrmms.2011.09.018.
Xu, W.J., Hu, R.L. and Tan, R.J. (2007), "Some geomechanical properties of soil-rock mixtures in the hutiao gorge area, China", *Geotechnique*, **57**(3), 255-264. https://doi.org/10.1680/geot.2007.57.3.255.
Yang, S.L., Lacasse, S. and Sandven, R.F. (2006), "Determination of the transitional fines content of mixtures of sand and non-plastic fines", *Geotech. Test J.*, **29**(2), 102-107. https://doi.org/10.1520/GTJ14010.
Yideti, T.F., Birgisson, B., Jelagin, D. and Guarin, A. (2013), "Packing theory-based framework to evaluate permanent deformation of unbound granular materials", *Int. J. Pavement Eng.*, **14**(3), 309-320. https://doi.org/10.1080/10298436.2012.736620.
Yin, Z., Zhao, J. and Hicher, P. (2014), "A micromechanics-based model for sand-silt mixtures", *Int. J. Solids Struct.*, **51**(6), 1350-1363. https://doi.org/10.1016/j.ijsolstr.2013.12.027.
Yu, A.B. and Standish, N. (1988), "An analytical-parametric theory of the random packing of particles", *Powder Technol.*, **3**(55), 171-186. https://doi.org/10.1016/0032-5910(88)80101-3.
Zhang, J. and Yang, J. (2017), "Experimental and numerical investigation of dilation behavior of asphalt mixture", *Int. J. Geomech.*, **17**(2). https://doi.org/10.1061/(ASCE)GM.1943-5622.0000738
Zhou, W., Xu, K., Ma, G., Yang, L. and Chang, X. (2016), "Effects of particle size ratio on the macro- and microscopic behaviors of binary mixtures at the maximum packing efficiency state", *Granul. Matter*, **18**(4), 1-13. https://doi.org/10.1007/s10035-016-0678-1.

JS